Article

Mechanochemical Synthesis and Three-Dimensional Electron Diffraction Structure Solution of a Novel Cu-Based Protocatechuate Metal−Organic Framework

Andrea Sala, Moussa D. Faye Diouf, Danilo Marchetti, Lea Pasquale, and Mauro Gemmi*

Read Online

ACCESS | Metrics & More | Article Recommendations | SI Supporting Information

ABSTRACT: Mechanochemical synthesis is a powerful approach to obtain new materials, limiting costs, and times. However, defected and submicrometrical-sized crystal products make critical their characterization through classical single-crystal X-ray diffraction. A valid alternative is represented by three-dimensional (3D) electron diffraction, in which a transmission electron microscope is used, like a diffractometer. This work matches a green water-based mechanochemical synthesis and 3D electron diffraction to obtain and characterize a Cu-based protocatechuate metal−organic framework (PC-MOF). Its structure has been fully refined through dynamical diffraction theory, and free water molecules could be detected in the channels of the framework. Thermal characterization, focused on the dehydration profile determination, leads to the formation of a novel high-temperature 2D coordination polymer, fully solved with 3D electron diffraction data. At last, the strong activity of the PC-MOF against cationic dyes like methylene blue has been reported.
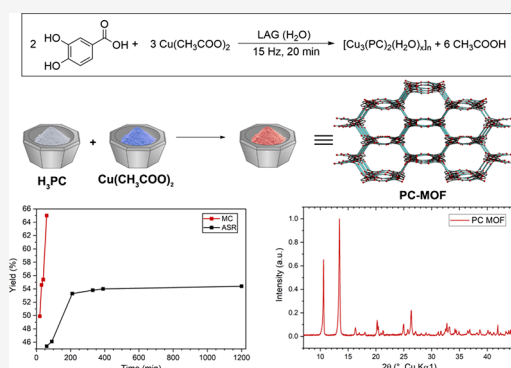
INTRODUCTION

Metal−organic frameworks (MOFs) are a class of porous materials heavily studied in the past decades.[1−3] The reason for a similar interest should be retrieved in the enormous number of applications like energy storage,[4] sensing,[5] drug delivery,[6] water purification,[7,8] catalysis,[9] gas sorption, or separation.[10] In recent years, few studies have moved forward to a new generation of bio-MOFs. The aim is to use bioactive molecules as ligands such as active pharmaceutical ingredients (API)[11] or plant-extracted biomolecules.[12,13] Overall, symmetric ligand molecules are generally required to synthesize MOFs and the most common synthesis is represented by solvothermal methods. Those involve undoubtedly the use of large amounts of energy, time, and toxic chemicals, even for the preparation of small quantities of products, with a scarce consideration of the sustainability facets. An emerging, potentially green, and sustainable alternative synthesis method is nowadays represented by mechanochemistry (MC).[14−16] Initially employed as a homogenization technique for material blending, MC has been rediscovered to be a powerful low-cost technique that involves low synthetic energies and reduces chemical wastes, maintaining at the same time a high conversion ratio.[17] The basic principle of MC synthesis consists of the absorption of mechanical energy to induce reactions between reagents in the solid state. The impacts and frictions on reagent powders create very defective, thus reactive, crystalline domains leading to kinetically governed solid state reactions. Depending on experiments and equipment, solids, liquids, and even reactive

gases could be employed in an MC reaction.[18] Nevertheless, the most common processes are represented by neat grinding (NG) and liquid-assisted grinding (LAG) in which powders are, respectively, treated dry or homogenized in the presence of a liquid additive. Solvents can heavily influence the synthesis, even if not reactive.[19]

Very frequently, the yield of a MC reaction, besides being multiphasic, is constituted by products of poor crystal quality with monocrystalline domains smaller than a few microns. Consequently, the structural characterization of MC synthesized samples is a true challenge since single-crystal X-ray diffraction (SC-XRD) cannot be performed, and powder X-ray diffraction is usually poorly informative (with only a few peaks and the problem of peak overlapping from multiple phases). To exploit the undoubtable advantages of MC without a critical lack of knowledge on the products of synthesis, a structural characterization technique efficient in the nanocrystalline domain should be found. 3D electron diffraction (3D ED) is a possible choice.[20] Exploiting the stronger interaction of electrons with matter (from 3 to 4 orders of magnitude more than X-ray in amplitude), it is possible to
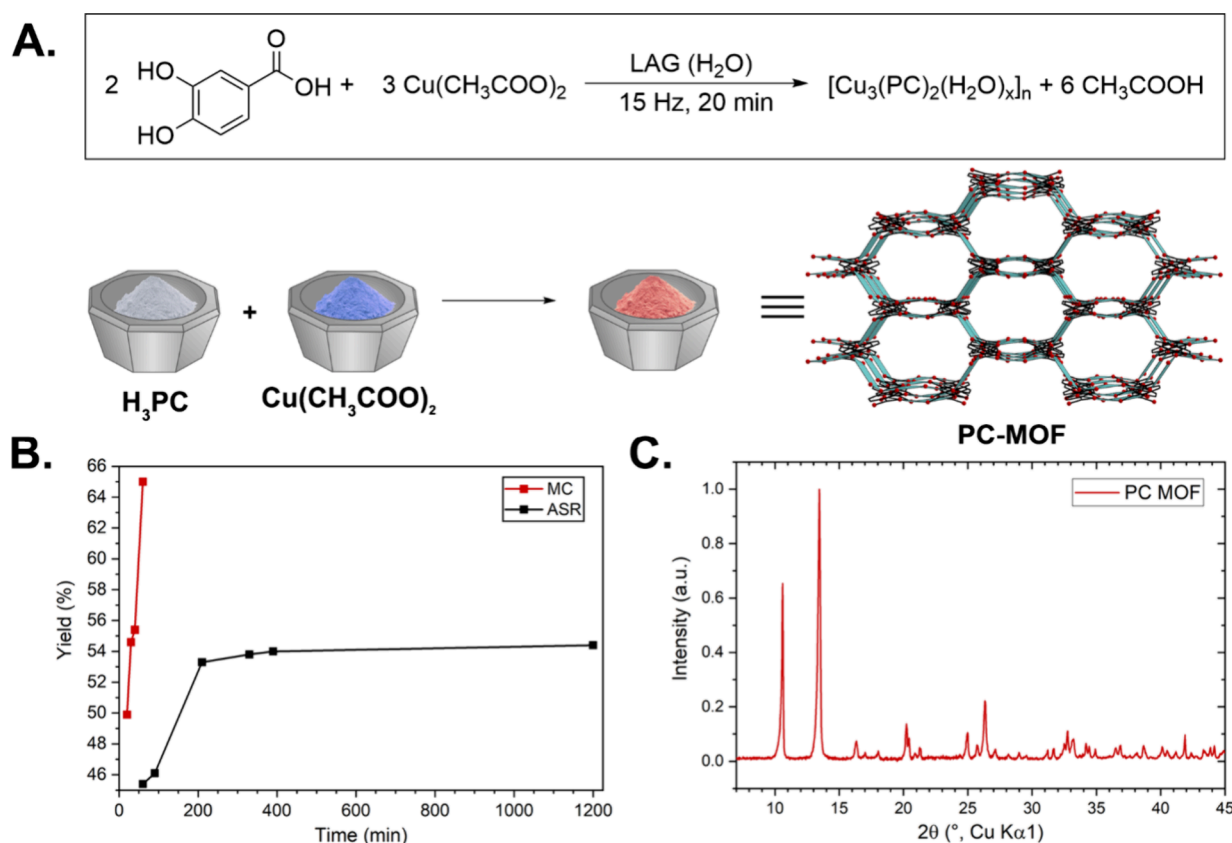
Figure 1. (A) Schematic representation of the mechanochemical reaction followed for the PC-MOF synthesis. (B) Comparison of the yield over time for the two synthetic methods, highlighting the better performance of MC with respect to ARS synthesis. (C) PXRD pattern of the mechanochemically synthesized PC-MOF, with the intensity values normalized to the maximum peak.

collect 3D ED single-crystal data on crystalline grains as small as a few hundreds of nanometers. The experiment is like a classical SC-XRD data collection. Herein, the diffractometer is substituted by a transmission electron microscope (TEM) in which the electron beam is directed onto a nanocrystal, which can be carefully selected by exploiting the imaging capabilities of the TEM. Literally, a crystal search is performed, and the crystal quality can be checked through a preliminary single-shot diffraction. If the crystal quality is acceptable, as in SC-XRD, then the sample is rotated through a goniometer and the diffraction patterns are collected in sequence with an area detector.[21] MOFs are usually very beam-sensitive and can be easily amorphized by the electron beam; therefore, the experiment must be carried out in low illumination mode with total electron doses smaller than 1 el Å^{-2}. In this case, the use of a single-electron hybrid detector is recommended for recording acceptable diffraction signals.[22] The peculiar diffraction geometry of each pattern, most of the time far from zone axis conditions, guarantees that the 3D ED intensities can be successfully used in a structure solution attempt as the squared modulus of the structure factors (kinematical approximation). The structure can also be refined either within the kinematical approximation scheme or, to a higher level of accuracy, taking into account the residual dynamical scattering,[23] if the data quality allows it. 3D ED has been successfully applied to the structure determination of a variety of beam-sensitive materials like coordination polymers,[24] cocrystals,[25] APIs,[26] proteins,[27] or MOFs.[28]

In this work, we demonstrate a fast and green mechanochemical synthesis of a MOF based on protocatechuic acid and copper (PC-MOF) and its full structure determination by 3D ED analysis. Protocatechuic acid (H$_3$PC; 3,4-dihydroxybenzoic acid)[29] is a very interesting molecule due to its wide bioavailability in nature and in common edible plants like onions, brown rice, or gooseberries. Moreover, this phenolic acid is a validated and strong antioxidant,[30] antiflammatory,[31] and antitumoral substance.[32] Copper acetate monohydrate (Cu(OAc)$_2$·H$_2$O) was chosen as the metal source due to the strong activity of copper in antimicrobial applications[33] and pollutant degradation.[34]

The possibility of obtaining a PC-MOF has already been demonstrated. However, the only explored synthesis route is a classical solvothermal using *N,N*-dimethylformamide (DMF) as the solvent, which results to be coordinated to the MOF framework in its structure.[35] Herein, we demonstrate the possibility of substituting this synthesis route with a green mechanochemical approach that leads to a solvent-free PC-MOF with only water in its pores. In addition, complete structural and thermal characterization has been carried out with a specific focus on the dehydration profiles and consequent reorganization of the structure. Finally, the PC-MOF has shown remarkable activity in pollutant sorption from water. The target molecule in our study is methylene blue, a common chemical extensively used in medicine and as a textile dye.[36]

RESULTS AND DISCUSSION

Synthesis. To synthesize the Cu (II)-based PC-MOF using a rapid, harmless, and eco-friendly approach, we focused on mechanochemical synthesis (Figure S1), conducted through a

LAG reaction employing water as additive. The reaction takes place in a few minutes of milling thanks to the tiny volume of liquid employed in the LAG process, which enhances the reagent diffusion during the experiment. As a reference, we also tested the PC-MOF synthesis by performing a reaction into aqueous solution (aqueous solution reaction, ASR; Figure S2). This method is still capable of delivering the PC-MOF as a product with a definitely lower yield than the MC approach. It must be recalled that during the MC reaction, the acetic acid released by the PC-MOF formation could not be completely solubilized in the liquid additive. This allows a partial release of this subproduct in the surrounding atmosphere, pushing the MC reaction toward the formation of the desired framework in a few minutes (Figure 1A). This plays an important role in the enhancement of the MC reaction as well as total yields, with respect to the ASR method.[37] After 60 min of stirring, the ASR method led to a 45.4% yield, which rises to 46.1% after 90 min and to 54.4% if the suspension is stirred overnight. Oppositely, in only 20 min of milling, the MC method led to a 49.9% yield, which rises to 55.4% in 40 min and to 65.0% in only 60 min (Figure 1B).

The formation of the desired network was confirmed through spectroscopy and diffraction techniques. The IR spectra (Figure S25) confirmed the absence, in the MC reaction crude, of both acetic acid and typical peaks of protonated carboxylic acids (e.g., ~1663 cm^{-1}). In Figure 1C, this instead reports the PXRD pattern of the same sample, which shows a nice crystallinity of the product. Herein, it is clear that something new has formed since this pattern cannot be indexed with any of the reagent structures.

The obtained compound has been found to be very stable under different solvent conditions. To test its stability, different batches of powder were inserted in different liquids (organic solvents and aqueous solutions) for 3 days. The crystalline phase was not modified by the presence of different liquid media except in the presence of DMF, in which the resulting PXRD pattern matches with the $[Cu_3(PC)_2(DMF)_2]_n$ phase (Figure S3).[35]

Structure Determination. The crystal structure of the synthesized PC-MOF powder was investigated through a 3D ED analysis. This characterization technique is perfectly suitable for the MC product due to its nanosize and well-diffracting crystals (Figure S4). The 3D ED experiment was done in a Zeiss Libra 120 TEM, operating at 120 kV, able to work in a special low dose mode (i.e., below 0.05 el s^{-1} Å^{-2}) and equipped with a Timepix single-electron detector.[21] The 3D ED data have been collected in continuous rotation mode (cRED) on four crystals at a temperature of 293 K. The obtained electron diffraction data were processed and indexed with PETS2.0 software.[38] All the collected data sets could be indexed with a C-centered monoclinic cell with parameters a = 21.171(7) Å, b = 7.005(3) Å, c = 16.903(6) Å, and β = 127.23(2)°. Its symmetry was determined by checking the systematic absences from the 2D sections of the reciprocal lattice (Figure S6). Reflection conditions for hkl and $0kl$ sections are h, l = 2n, and $h + k$ = 2n, consistent with the extinction symbol $C1c1$, thus space groups Cc and $C2/c$. The structure solution was obtained *ab initio* on a single cRED data set (see Table S1) in the space group $C2/c$ using SHELXT,[39] localizing all non-H atoms of the MOF's framework.

A kinematical refinement of the initial model converged to an R(obs) of 27.91%. Residual electrostatic potential in the channels of the structure suggests the presence of trapped

water molecules. However, the determination of their positions remains elusive during the kinematic refinement process. Subsequently, we carried out a refinement approach employing the dynamical diffraction theory[36] using the JANA2020 software package.[40] This results in a substantial reduction of the R-factor, from 27.91 to 11.75%. The dynamical refinement process yielded a significantly more interpretable electrostatic potential, enabling the unambiguous identification of all hydrogen positions, despite their low scattering power (Figure S10A). Moreover, a pronounced residual peak observed in the Fourier difference map could be attributed to an oxygen atom, likely originating from a water molecule (Figure S15A). The refinement of this position and its thermal parameter is unstable; therefore, we modeled it with two split sites partially occupied. The occupancies of the two water positions are refined to 0.188 and 0.189, which give 0.75 water molecules per formula unit.

The asymmetric unit of the PC-MOF is composed of a single PC^{3-} molecule, two copper atoms, and a partially occupied water molecule (Figure S8). This arrangement involves two distinct copper atoms, one in a general position (Cu1) and the other in a special position (Cu2), both displaying a square planar coordination geometry. The deprotonated carboxyl group establishes distinct coordination interactions with individual copper atoms, in which each oxygen acts as a monodentate ligand toward Cu1 or Cu2. Furthermore, the catecholate group plays a dual role in performing bidentate chelation on Cu1 while O3 and O4 are acting as bridging sites, respectively, on Cu1(1-*x*, *y*, 3/2-*z*) and Cu2 (Figure S11A). The connection of four molecules of H$_3$PC leads to a dimeric cluster, in which Cu1 and Cu1(1-*x*, *y*, 3/2-*z*) atoms are involved in a distorted square planar coordination geometry, with their corresponding polyhedra sharing one edge (Figure S11B). This gives rise to a corrugated double chain that extends along the [101] direction (Figure 2A), with a corrugation angle of 149.8° (Figure S13). The Cu2
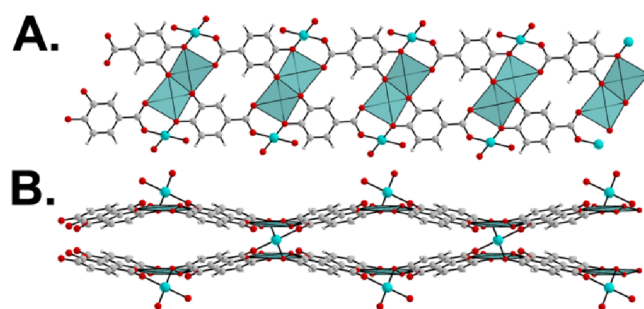

Figure 2. Representations of the PC-MOF framework's portions, to highlight its peculiar connectivity. (A) Polymeric corrugated double chains of PC^{3-} and Cu1, oriented along the crystallographic *b* axis. (B) Simplified view of two chains connected by Cu2 and oriented along the *c* axis. The Cu1 atoms are represented as turquoise polyhedra, while Cu2 atoms are represented as spheres.

atom, which is in a crystallographic special position, is involved in a square planar coordination geometry sharing one vertex with the Cu1 and Cu1(1-*x*, 1-*y*, 1-*z*), acting as a bridge between the corrugated double chains (Figure 2B) and resulting in the formation of a 3D framework with the formula $\{[Cu_3(PC)_2](H_2O)_{0.75}\}_n$ (Figures 3A and 4). The obtained framework is characterized by channels running along the [101] direction, whose walls are made by two opposite
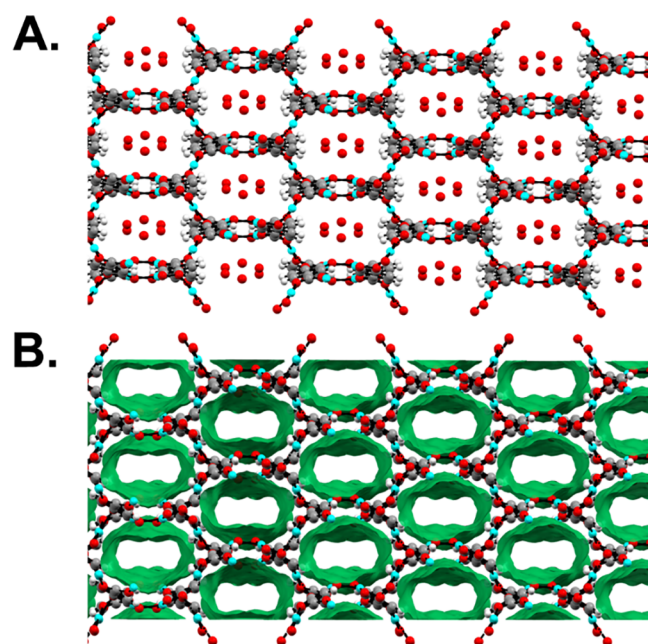
Figure 3. (A) Crystal structure oriented along the [101] direction and (B) representation of the calculated virtual voids. The accessible surface area is displayed in green with carbon atoms in gray, oxygens in red, hydrogen in white, and copper in turquoise.
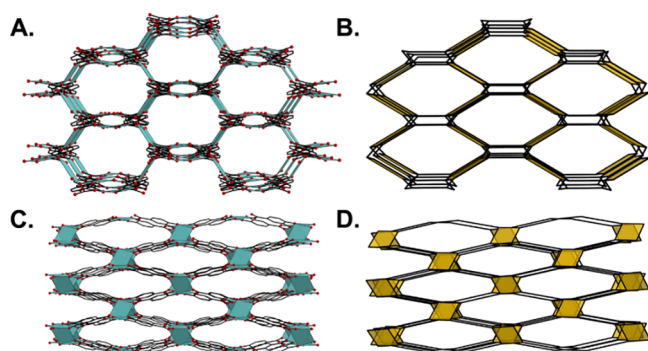

Figure 4. View of the PC-MOF structure oriented along (A) [001] and (C) [101]. On the right side, panels (B, D) represent the corresponding simplified nets, calculated through the point of extension method.[42] Solvent molecules and hydrogen atoms have been omitted for clarity.

corrugated chains laterally connected by four Cu2 square planar polyhedra leaving a distorted hexagonal section, and it displays 39.2% of unit cell volume as a virtual void (Figure 3B). Theoretical calculations, performed with Mercury,[41] highlight the presence of pore diameters of around 3.90 and 4.33 Å, with a total surface area of $\sim$119.53 m^2 g^{-1}. The network simplification led to a (3,4)-c net characterized by the point symbol {4.6.8} {4.6^2.8^3} (Figure 4 and Figure S24).

Comparing our PC-MOF structure with the previously reported $[Cu_3(PC)_2(DMF)_2]_n$, the most striking contrast emerges in the coordination geometry of the two copper atoms due to the coordination of the DMF molecule to the metal centers. In $[Cu_3(PC)_2(DMF)_2]_n$, Cu1 adopts a square pyramid coordination geometry, while Cu2 exhibits an octahedral coordination. On the other hand, in $\{[Cu_3(PC)_2](H_2O)_{0.75}\}_n$ structure, both copper atoms assume a distorted square planar coordination environment and the water in the channel does not coordinate the metals.

Additionally, a variance in the corrugation angle is also observed. The $[Cu_3(PC)_2(DMF)_2]_n$ structure exhibits a slightly smaller corrugation angle of 133.2°.

The fact that two structures with the same framework topology exhibit such variability highlights the PC-MOF's flexibility, capable of altering its lattice in response to specific guest molecules.

The PC-MOF structural model, obtained from the 3D ED analysis, was then refined with the Rietveld approach against the PXRD data of the mechanochemically synthesized product (Figure S14). This refinement highlights a slight variation of the lattice parameters, a = 20.813(3) Å, b = 7.1431(5) Å, c = 16.9679(15) Å, and β = 126.935(6)°. This unit cell parameter change could be correlated to the desorption of guest molecules embedded in the MOF cavities promoted by the high vacuum inside the TEM ($\sim$10^{-9} bar). The 3D ED structure would be an almost empty PC-MOF, while the one observed in PXRD is filled with water. This is confirmed by the Rietveld refinement of the 3D ED model, which shows a strong underestimation of the first peak at 10.61°. This peak is sensitive to the channel occupation, as can be seen by calculating the pattern from a completely empty model where the peak is much weaker (Figure S16). The loading of the PC-MOF can be verified also from the Fourier difference map calculated on the PXRD refined model, in which a broad electron density map fills the channels (Figure S15). Unfortunately, the disorder of the water in the channels prevents any refinement of their position through a Rietveld approach. Nevertheless, as discussed before, the 3D ED analysis, followed by a dynamical refinement, allowed us to easily locate the adsorbed solvent molecules. The result further highlights the power of the dynamical refinement with 3D ED data.[43]

Thermal Behavior. To detect what is the fate of the PC-MOF once the channels are fully empty, we studied its thermal behavior and the way the water is lost during heating.

We performed a temperature-resolved *in situ* PXRD analysis with the sample packed into an open capillary with a ramp from room temperature to 155 °C (Figure 5A). This experiment revealed, around 100 °C, a rapid change of the PXRD profile followed, at the end of the experiment, by a wide reduction of its crystallinity. A Le Bail fit revealed a standard thermal expansion in the first part followed, around 110 °C, by a sharp reduction of the b axis (Figure 5B). This is a clear consequence of the pore contraction due to solvent loss, as can be inferred by comparing the $\{[Cu_3(PC)_2](H_2O)_{0.75}\}_n$ and $[Cu_3(PC)_2(DMF)_2]_n$ structures. The MOF loaded with DMF, a larger guest, has a much longer b parameter compared to the PC-MOF.

If rapidly heated in an open system (i.e., a porcelain crucible at 150 °C for 60 min) with a wider aperture than a capillary, then the PC-MOF undergoes an irreversible phase transition leading to a new crystalline phase. The IR spectrum confirms the absence of any molecular degradation or reaction (Figure S26). The latter, very similar to PC-MOFs, differs only in the absence of a broad water peak at 3000−3600 cm^{-1}. The rapid heating in a totally open setup leads to a dreadful PXRD pattern (Figures S17 and S18), in which only a few peaks are clearly identifiable in the huge, amorphous background. At first glance, the PXRD pattern is not informative, and the PC-MOF should be considered completely amorphized. An inspection of the sample in the TEM shows a different scenario: a new high-temperature (HT) phase can be detected and solved. The
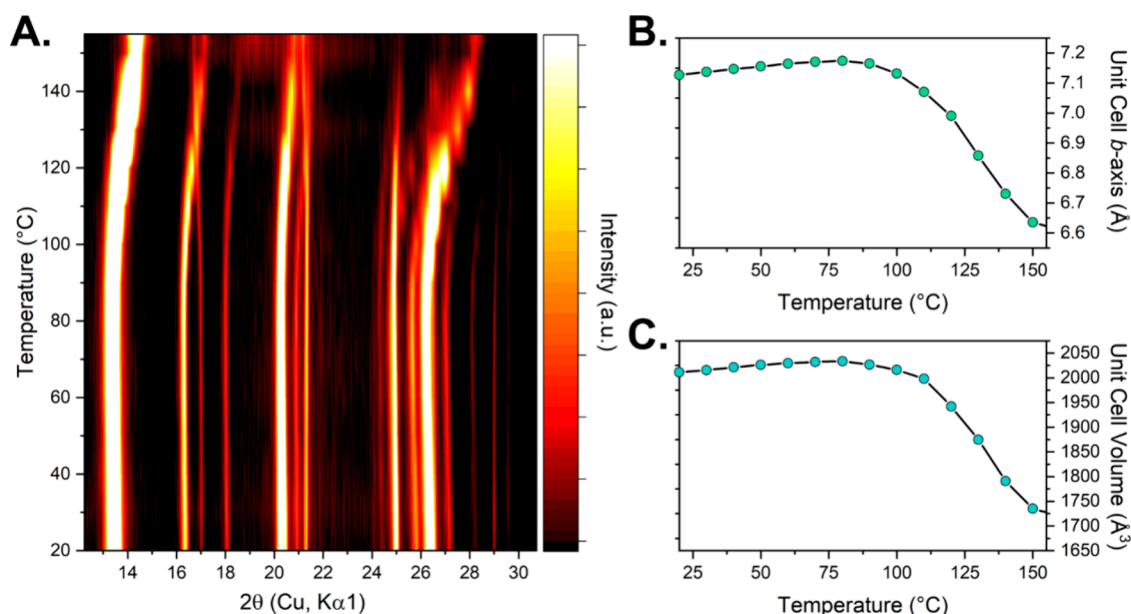
Figure 5. Temperature-induced phase transition of the PC-MOF analyzed by temperature-resolved *in situ* powder X-ray diffraction. (A) 2D projection along the intensity axis of the powder diffractograms. (B, C) Unit cell *b* axis and volume values resulted from the Le Bail refinement conducted on each collected diffraction pattern. For clarity reasons, we reported only the *b* axis and the cell volume since they are the most affected by the framework contraction induced by solvent removal.
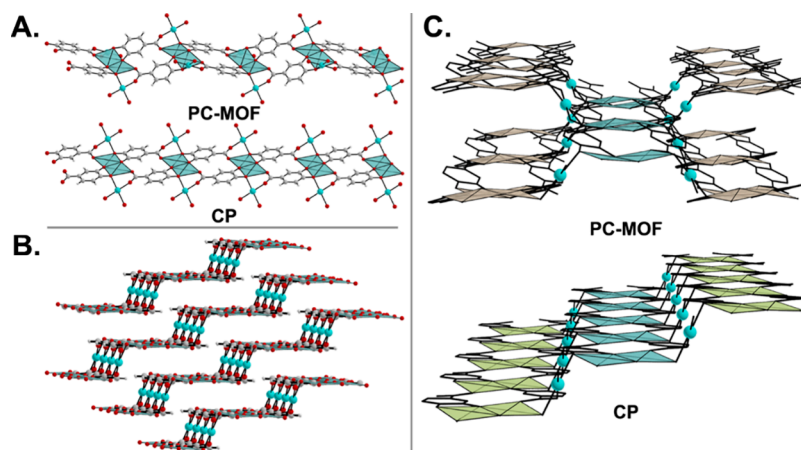

Figure 6. (A) Comparison of the double-chain structure in the CP and PC-MOF, (B) role of the different copper atoms in the CP structure, and (C) view of the layered staircase structure growing along [110].

crystal structure was fully determined by 3D ED characterization, performed with the same instrumental setup and conditions described for the PC-MOF. Despite the presence of multiple reflections belonging to different crystals during data acquisition, data reduction was carried out successfully with PETS2. This HT structure exhibits a triclinic cell of $a = 5.4032(19)$ Å, $b = 7.404(2)$ Å, $c = 8.7168(15)$ Å, $\alpha = 73.656(17)°$, $\beta = 88.24(2)°$, and $\gamma = 82.24(2)°$, and the *ab initio* structure solution highlighted the presence of a two-dimensional coordination polymer (CP), see Table S1. Dynamical refinement was also carried out on the CP, resulting, as expected, in an important drop in the *R*-factor, from 33.35% upon kinematical refinement down to 16.35%. Hydrogen positions could be easily localized in the electrostatic potential (Figure S10B).

The asymmetric unit of the CP is constituted by a single PC^{3-} unit and two copper atoms (Figure S9) with the overall unit cell consisting of two PC^{3-} molecules and three copper

atoms since, also in this case, one of the copper atoms is in a special position. The building units of the CP are the same as described earlier for the PC-MOF. In contrast to the latter, where the bonding of four molecules of H_3PC yields a corrugated layer, in the CP, the bonding to a dimeric square planar cluster of Cu1 atoms results in a double-chain structure with flat geometry along the [001] direction (Figure 6A and Figure S13), characterized by slipped layers, where each layer is slightly shifted relative to the adjacent layers during stacking while keeping a constant distance of 3.106 Å. The Cu2 atom continues to occupy an inversion center, serving as a bridge between the different layers. Notably, like the previously mentioned structures, both Cu1 and Cu2 exhibit distorted square planar geometries. However, the key distinction lies in the coordination environment of Cu2, which is extended only along two dimensions. As a result, a distinctive layered staircase-like structure is formed, wherein the layers are
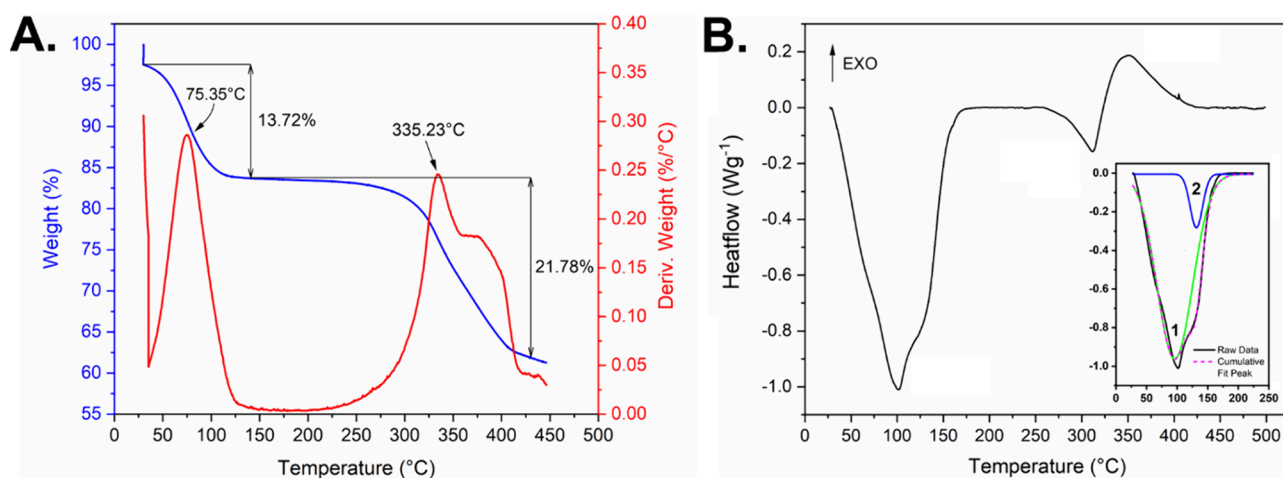
Figure 7. Thermal characterization of the PC-MOF and CP. (A) TGA curve until 500 °C, completed by loss percentages and derivatives. (B) DSC thermogram until 500 °C and deconvolution detail of the dehydration peak (exothermic peaks up).

connected in a 2D manner and exhibit stepwise growth along the [110] direction (Figure 6B,C).

Since PC-MOF and CP structures have been kinematically and dynamically refined, we compared the obtained results in terms of bond length and atomic position absolute differences. Taking into consideration the standard values reported in literature,[44,45] the average difference between tabulated and refined values is calculated for every structure refined in this work. For the PC-MOF, the average differences in bond length are 0.01811 for dynamical refinement and 0.02521 for kinematical refinement. This points out the goodness of the dynamical approach over the kinematical refinement for the PC-MOF. On the contrary, this is not achieved for the CP due to poor data quality. In this case, the difference between the two refinement methods is negligible. All details for bond length differences and analysis of atomic positions are reported in the Supporting Information (Paragraph S3.3).

A complete thermal characterization of the PC-MOF is reported in Figure 7. Thermogravimetry analysis (TGA) and differential scanning calorimetry (DSC) have been performed up to 450 and 500 °C, respectively (Paragraph S6). As specified above, through dynamical refinement, 0.75 water oxygens per asymmetric unit have been found. As evidenced by PXRD data analysis, this value is highly underestimated due to TEM's high vacuum. Calculated structural analysis in Mercury suggested that the pore diameter could accommodate up to four water molecules per formula unit, occupying two independent sites. Despite this, the susceptivity to experimental conditions like pressure, combined with disorder, and the above-mentioned structural flexibility makes this evaluation very critical. In addition, the dried PC-MOF's powders present a strong hygroscopic behavior, leading to a possible water overestimation in thermal analysis. This is the case of the TGA curve in Figure 7A where the estimated amount of the trapped solvent at an ambient pressure of 1 atm is equal to 13.72% of the sample's total weight (the peak maximum is retrievable at 75.35 °C). From this percentage, an overestimated value of 2.5 water molecules per asymmetric unit can be calculated. Obviously, there is no signature of the CP formation in TGA, while CP degradation starts to be seen above 300 °C with a peak in the derivative at 335 °C, accompanied by a weight loss of 22%. In the DSC thermogram, as reported in Figure 7B, the first endothermic peak is correlated to PC-MOF

dehydration and the simultaneous CP formation. Indeed, it appears clear that this asymmetric peak is composed of an overlap of different contributions with a minimum at 101.4 °C. The resulting peak is the result of a complex dehydration process that, if described as the deconvolution of two major signals, only gives one major peak at 96 °C and a second one at 131.1 °C, which can be associated with water loss processes and CP phase formation, respectively. The transition from PC-MOF to CP has been found to be irreversible (Figure S27).

Although the thermal analysis has revealed that the PC-MOF does not exist in an empty activated form, its high stability in different solvents allowed us to valorize this material. The preliminary study herein reported is only the first experimental evidence of a more extensive work, currently underway, focused on the selective sorption of cationic pollutants from water.[46] A large class of wastes, often forgotten, is represented by textile dyes. Their very high solubility in water makes the purification of aqueous systems somewhat difficult.[47] As a possible proof of concept, we selected as the target methylene blue (MB): one of the most common synthetic dyes used not only in fabric coloration but also in food additives, cosmetics, and pharmaceutical industries.[48] All experimental details and observations are reported in the Supporting Information, Paragraph S7.

The removal efficiency ($R\%$) and amount of adsorption q_e (mg/g) over time clarify the strong PC-MOF activity toward MB at low concentrations (Figure 8A). In 5 min only, a $R\%$ of 61.7% is reached, and it is further increased to 73.1% in the next 15 min (i.e., 20 min in total). The overall $R\%$ corresponds to 75.2% in 90 min and q_e to 37.61 mg/g. Standard deviations for this plot are reported in Table S7. Figure 8B reports the superimposition of the UV−vis scans for the uptakes at various time intervals. The reason for the uptake curve flattering as well as UV−vis signal broadening and shift from 663 to 678 nm is fully described in Paragraph S7 and Figure S28B. The comparison of the PXRD patterns of pure and MB-treated PC-MOF's powders demonstrates that the structure is not affected by the dye's treatment (Figure 8C). This suggests that MB is only absorbed on the MOF's surface. Last, Figure 8D shows the color changes of both MB solutions and PC-MOF powders before and after the treatment. It is possible to notice the decoloration of the solution and the bluish aspect of treated powders.
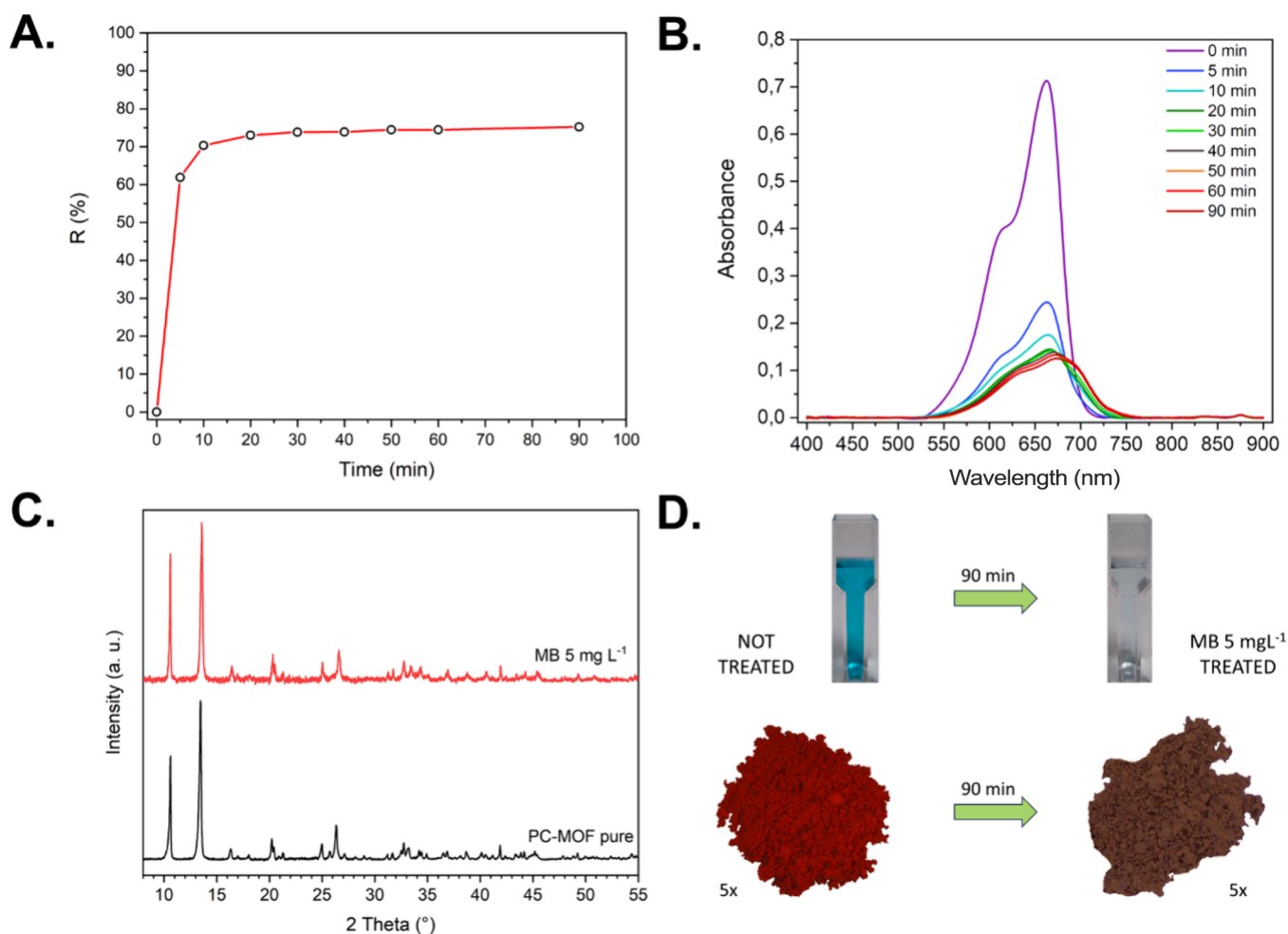
A.

B.

C.

D.

Figure 8. MB uptake experiments. (A) Removal percentage of MB over time given an initial concentration of 5 mg L^{-1}. (B) Series of UV−vis spectra collected at various times of the experiment. (C) PXRD pattern comparison between the pristine and treated powder. (D) Comparison of MB solutions and PC-MOF sample color before and after MB treatment. Powder's images have been collected through an optical stereomicroscope (5× magnification).

To compare the effects given by thermal treatment, the same MB uptake experiments have been carried out also on the CP. The loss of porosity plays an important role, and the CP turns out to be less efficient than the PC-MOF while maintaining a very similar behavior (Figure S29 and Table S8). Furthermore, PC-MOF-treated powders have been analyzed through energy-dispersive spectroscopy (EDS) to distinguish the MB presence on grain surfaces. The EDS spectra of pure and MB-treated PC-MOF are reported in Figures S30 and S31, respectively. The sulfur peak at 2.3 keV has been chosen as the target and discriminant to demonstrate whether dye uptake was successful. At last, some release tests were performed in pure Milli-Q water at a pH of 7.0 ± 0.1. The study, reported in the Supporting Information (Paragraph S7.1), indicates the possibility to remove a moiety of the absorbed dye, slightly varying the pH value of the system. In 180 min, the PC-MOF and CP release 23.29 and 17.94% of their previously absorbed MB, respectively (Figure S32 and Table S9).

■ CONCLUSIONS

In summary, we reported the fast and eco-friendly synthesis through mechanochemical (MC) liquid-assisted grinding (LAG) of a Cu-based protocatechuate MOF (i.e., PC-MOF). The innovative approach turned out to be superior to common

methods such as aqueous solution reaction (ASR) or solvothermal synthesis in terms of yield of the final product. Although the PC-MOF was nanocrystalline (the grains were usually smaller than 1 μm), the structure could be solved through 3D electron diffraction (3D ED) and dynamically refined, obtaining a R% of 11.75%. In addition, the ligand's hydrogen atoms as well as water molecules have been successfully refined. Remarkably, the PC-MOF presents a 3D lattice in which water molecules are trapped and are not coordinated with metal nodes. This totally differs from a similar structure synthesized via the solvothermal method using *N,N*-dimethylformamide as the solvent.[35] The PC-MOF structure is flexible and stable in several organic solvents or aqueous solutions at different pH. The MOF was also extensively characterized. Very accurate thermal and spectroscopic studies (i.e., time-resolved PXRD *in situ*, TGA, DSC, and FTIR-ATR) revealed that it is not possible to remove water without incurring the collapse of the structure with the formation of a 2D coordination polymer (CP). The presence of this high-temperature degradation phase was completely unexpected since the PXRD pattern of the thermally treated powder was really poor with a dominant contribution from an amorphous phase. Remarkably, inspection of the sample with 3D ED allowed the detection of a nanocrystalline product (i.e.,

CP) and its full structure determination. This confirms that 3D ED is a powerful tool also for the detection of elusive nanocrystalline products, which can escape standard screening investigations.

To better understand the phase transition related to water loss, an accurate cross-referencing of all thermal data helped us to define the PC-MOF's dehydration process as continuous, leading to the complete collapse of the structure and the impossibility to activate it. Despite this limit, the possibilities of application are still wide. In the previous work, $[Cu_3(PC)_2(DMF)_2]_n$, after a solvent exchange with ethanol, has shown a newsworthy antimicrobial activity. In this work, we focused on a broader application field, such as the selective sorption of cationic pollutants from water. The PC-MOF proved to be efficient toward a cationic textile dye as methylene blue (MB) at low concentrations at pH 7.4. MOF's pores are not permeated, but the sorption takes place only on grain surfaces. This result was confirmed through energy-dispersive spectroscopy (EDS). In addition, preliminary release studies have been reported, slightly modifying the pH to 7.0. Further studies are ongoing to establish the pH influence on the systems reported above and the adsorption of the different cationic pollutants.

■ ASSOCIATED CONTENT

ⓈⒾ Supporting Information

The Supporting Information is available free of charge at https://pubs.acs.org/doi/10.1021/acs.cgd.3c01494.

> The supporting information contains: details on the synthesis procedures; stability test of the PC-MOF in different solvents; tables with crystallographic details of the two structures; details of the 3D ED data collection procedure; different pictures describing the crystal structures; details on the powder diffraction experiments and the 3D ED structural refinements; details on the topological analysis; a complete summary of the spectroscopic and thermal analysis; a complete description of the dye release and absorption tests (PDF)

Accession Codes

CCDC 2313885 and 2313891 contain the supplementary crystallographic data for this paper. These data can be obtained free of charge via www.ccdc.cam.ac.uk/data_request/cif, or by emailing data_request@ccdc.cam.ac.uk, or by contacting The Cambridge Crystallographic Data Centre, 12 Union Road, Cambridge CB2 1EZ, UK; fax: +44 1223 336033.

■ AUTHOR INFORMATION

Corresponding Author

Mauro Gemmi − *Electron Crystallography, Istituto Italiano di Tecnologia, Pontedera 56025, Italy;* ⓘ orcid.org/0000-0001-9542-3783; Email: mauro.gemmi@iit.it

Authors

Andrea Sala − *Electron Crystallography, Istituto Italiano di Tecnologia, Pontedera 56025, Italy;* ⓘ orcid.org/0000-0001-7265-9187

Moussa D. Faye Diouf − *Electron Crystallography, Istituto Italiano di Tecnologia, Pontedera 56025, Italy; Dipartimento di Scienze Chimiche, della Vita e della Sostenibilità Ambientale, University of Parma, Parma 43123, Italy;* ⓘ orcid.org/0000-0003-0862-3272

Danilo Marchetti − *Electron Crystallography, Istituto Italiano di Tecnologia, Pontedera 56025, Italy; Dipartimento di Scienze Chimiche, della Vita e della Sostenibilità Ambientale, University of Parma, Parma 43123, Italy*

Lea Pasquale − *Materials Characterization Facility, Istituto Italiano di Tecnologia, Genova 16163, Italy;* ⓘ orcid.org/0000-0002-3919-8873

Complete contact information is available at:
https://pubs.acs.org/10.1021/acs.cgd.3c01494

Notes

The authors declare no competing financial interest.

■ ACKNOWLEDGMENTS

■ REFERENCES

(1) Udourioh, G. A.; Solomon, M. M.; Matthews-Amune, C. O.; Epelle, E. I.; Okolie, J. A.; Agbazue, V. E.; Onyeze, U. Current Trends in the Synthesis, Characterization and Application of Metal-Organic Frameworks. *Reaction Chem. Eng.* **2022**, 278−310, DOI: 10.1039/d2re00365a.

(2) Ding, M.; Cai, X.; Jiang, H. L. Improving MOF Stability: Approaches and Applications. *Chem. Sci.* **2019**, 10209−10230, DOI: 10.1039/c9sc03916c.

(3) Freund, R.; Zaremba, O.; Arnauts, G.; Ameloot, R.; Skorupskii, G.; Dincă, M.; Bavykina, A.; Gascon, J.; Ejsmont, A.; Goscianska, J.; Kalmutzki, M.; Lächelt, U.; Ploetz, E.; Diercks, C. S.; Wuttke, S. The Current Status of MOF and COF Applications. *Angew. Chem., Int. Ed.* **2021**, 23975−24001, DOI: 10.1002/anie.202106259.

(4) Baumann, A. E.; Burns, D. A.; Liu, B.; Thoi, V. S. Metal-Organic Framework Functionalization and Design Strategies for Advanced Electrochemical Energy Storage Devices. *Commun. Chem.* **2019**, 86 DOI: 10.1038/s42004-019-0184-6.

(5) Yuan, H.; Li, N.; Fan, W.; Cai, H.; Zhao, D. Metal-Organic Framework Based Gas Sensors. *Adv. Sci.* **2022**, 2104374 DOI: 10.1002/advs.202104374.

(6) Wu, M. X.; Yang, Y. W. Metal−Organic Framework (MOF)-Based Drug/Cargo Delivery and Cancer Therapy. *Adv. Mater.* **2017**, 1606134 DOI: 10.1002/adma.201606134.

(7) Xu, G. R.; An, Z. H.; Xu, K.; Liu, Q.; Das, R.; Zhao, H. L. Metal Organic Framework (MOF)-Based Micro/Nanoscaled Materials for Heavy Metal Ions Removal: The Cutting-Edge Study on Designs, Synthesis, and Applications. *Coord. Chem. Rev.* **2021**, No. 213554, DOI: 10.1016/j.ccr.2020.213554.

(8) Du, C.; Zhang, Z.; Yu, G.; Wu, H.; Chen, H.; Zhou, L.; Zhang, Y.; Su, Y.; Tan, S.; Yang, L.; Song, J.; Wang, S. A Review of Metal Organic Framework (MOFs)-Based Materials for Antibiotics Removal via Adsorption and Photocatalysis. *Chemosphere* **2021**, No. 129501, DOI: 10.1016/j.chemosphere.2020.129501.

(9) Wang, Q.; Astruc, D. State of the Art and Prospects in Metal-Organic Framework (MOF)-Based and MOF-Derived Nanocatalysis. *Chem. Rev.* **2020**, 1438−1511, DOI: 10.1021/acs.chemrev.9b00223.

(10) Li, J.; Bhatt, P. M.; Li, J.; Eddaoudi, M.; Liu, Y. Recent Progress on Microfine Design of Metal−Organic Frameworks: Structure Regulation and Gas Sorption and Separation. *Adv. Mater.*.20202002563. DOI: 10.1002/adma.202002563.

(11) Tibbetts, I.; Kostakis, G. E. Recent Bio-Advances in Metal-Organic Frameworks. Molecules. *MDPI AG* March 2, 2020. 251291.

(12) Grape, E. S.; Flores, J. G.; Hidalgo, T.; Martínez-Ahumada, E.; Gutiérrez-Alejandre, A.; Hautier, A.; Williams, D. R.; O'Keeffe, M.; Öhrström, L.; Willhammar, T.; Horcajada, P.; Ibarra, I. A.; Inge, A. K. A Robust and Biocompatible Bismuth Ellagate MOF Synthesized under Green Ambient Conditions. *J. Am. Chem. Soc.* **2020**, *142* (39), 16795−16804.

(13) Portolés-Gil, N.; Lanza, A.; Aliaga-Alcalde, N.; Ayllón, J. A.; Gemmi, M.; Mugnaioli, E.; López-Periago, A. M.; Domingo, C. Crystalline Curcumin BioMOF Obtained by Precipitation in Super-critical CO2 and Structural Determination by Electron Diffraction Tomography. *ACS Sustain Chem. Eng.* **2018**, *6* (9), 12309−12319.

(14) Głowniak, S.; Szczęśniak, B.; Choma, J.; Jaroniec, M. Mechanochemistry: Toward Green Synthesis of Metal−Organic Frameworks. *Mater. Today* **2021**, 109−124, DOI: 10.1016/j.mattod.2021.01.008.

(15) Tao, C. A.; Wang, J. F. Synthesis of Metal Organic Frameworks by Ball-Milling. *Crystals* **2020**, 15−20.

(16) Afshariazar, F.; Morsali, A. The Unique Opportunities of Mechanosynthesis in Green and Scalable Fabrication of Metal-Organic Frameworks. *J. Mater. Chem.* **2022**, 15332−15369, DOI: 10.1039/d2ta02059f.

(17) Pagola, S. Outstanding Advantages, Current Drawbacks, and Significant Recent Developments in Mechanochemistry: A Perspective View. *Crystals* **2023**, 124 DOI: 10.3390/cryst13010124.

(18) Bolm, C.; Hernández, J. G. Mechanochemie Gasförmiger Reaktanten. *Angew. Chem.* **2019**, *131* (11), 3320−3335.

(19) Yuan, W.; Friščič, T.; Apperley, D.; James, S. L. High Reactivity of Metal-Organic Frameworks under Grinding Conditions: Parallels with Organic Molecular Materials. *Angewandte Chemie - International Edition* **2010**, *49* (23), 3916−3919.

(20) Gemmi, M.; Mugnaioli, E.; Gorelik, T. E.; Kolb, U.; Palatinus, L.; Boullay, P.; Hovmöller, S.; Abrahams, J. P. 3D Electron Diffraction: The Nanocrystallography Revolution. *ACS Central Sci.* **2019**, 1315−1329, DOI: 10.1021/acscentsci.9b00394.

(21) Gemmi, M.; Lanza, A. E. 3D Electron Diffraction Techniques. *Acta Crystallogr. B Struct Sci. Cryst. Eng. Mater.* **2019**, *75*, 495−504.

(22) Nederlof, I.; Van Genderen, E.; Li, Y. W.; Abrahams, J. P. A Medipix Quantum Area Detector Allows Rotation Electron Diffraction Data Collection from Submicrometre Three-Dimensional Protein Crystals. *Acta Crystallogr. D Biol. Crystallogr.* **2013**, *69* (7), 1223−1230.

(23) Palatinus, L.; Corrêa, C. A.; Steciuk, G.; Jacob, D.; Roussel, P.; Boullay, P.; Klementová, M.; Gemmi, M.; Kopeček, J.; Domeneghetti, M. C.; Cámara, F.; Petříček, V. Structure Refinement Using Precession Electron Diffraction Tomography and Dynamical Diffraction: Tests on Experimental Data. *Acta Crystallogr. B Struct Sci. Cryst. Eng. Mater.* **2015**, *71*, 740−751.

(24) Marchetti, D.; Guagnini, F.; Lanza, A. E.; Pedrini, A.; Righi, L.; Dalcanale, E.; Gemmi, M.; Massera, C. Combined Approach of Mechanochemistry and Electron Crystallography for the Discovery of 1D and 2D Coordination Polymers. *Cryst. Growth Des* **2021**, *21* (12), 6660−6664.

(25) Sasaki, T.; Nakane, T.; Kawamoto, A.; Nishizawa, T.; Kurisu, G. Microcrystal Electron Diffraction (MicroED) Structure Determination of a Mechanochemically Synthesized Co-Crystal Not Affordable from Solution Crystallization. *CrystEngComm* **2023**, *25* (3), 352−356.

(26) Wang, Y.; Takki, S.; Cheung, O.; Xu, H.; Wan, W.; Öhrström, L.; Inge, A. K. Elucidation of the Elusive Structure and Formula of the Active Pharmaceutical Ingredient Bismuth Subgallate by Continuous Rotation Electron Diffraction. *Chem. Commun.* **2017**, *53* (52), 7018−7021.

(27) Clabbers, M. T. B.; Van Genderen, E.; Wan, W.; Wiegers, E. L.; Gruene, T.; Abrahams, J. P. Protein Structure Determination by Electron Diffraction Using a Single Three-Dimensional Nanocrystal. *Acta Crystallogr. D Struct Biol.* **2017**, *73* (9), 738−748.

(28) Huang, Z.; Grape, E. S.; Li, J.; Inge, A. K.; Zou, X. 3D Electron Diffraction as an Important Technique for Structure Elucidation of Metal-Organic Frameworks and Covalent Organic Frameworks.

Coord. Chem. Rev. **2021**, No. 213583, DOI: 10.1016/j.ccr.2020.213583.

(29) Kakkar, S.; Bais, S. A Review on Protocatechuic Acid and Its Pharmacological Potential. *ISRN Pharmacol* **2014**, *2014*, 1−9.

(30) Chou, T. H.; Ding, H. Y.; Lin, R. J.; Liang, J. Y.; Liang, C. H. Inhibition of Melanogenesis and Oxidation by Protocatechuic Acid from Origanum Vulgare (Oregano). *J. Nat. Prod* **2010**, *73* (11), 1767−1774.

(31) Masella, R.; Santangelo, C.; LiVolti, G.; Giovannini, C.; Galvano, F. Protocatechuic Acid and Human Disease Prevention: Biological Activities and Molecular Mechanisms. *Curr. Med. Chem.* **2012**, *19*, 2901 DOI: 10.2174/092986712800672102.

(32) Barahuie, F.; Hussein, M. Z.; Gani, S. A.; Fakurazi, S.; Zainal, Z. Synthesis of Protocatechuic Acid-Zinc/Aluminium-Layered Double Hydroxide Nanocomposite as an Anticancer Nanodelivery System. *J. Solid State Chem.* **2015**, *221*, 21−31.

(33) Vincent, M.; Hartemann, P.; Engels-Deutsch, M. Antimicrobial Applications of Copper. *Int. J. Hyg Environ. Health* **2016**, *219* (7), 585−591.

(34) Fang, L.; Liu, K.; Li, F.; Zeng, W.; Hong, Z.; Xu, L.; Shi, Q.; Ma, Y. New Insights into Stoichiometric Efficiency and Synergistic Mechanism of Persulfate Activation by Zero-Valent Bimetal (Iron/Copper) for Organic Pollutant Degradation. *J. Hazard Mater.* **2021**, No. 123669.

(35) Echenique-Errandonea, E.; Rojas, S.; Abdelkader-Fernández, V. K.; Pérez-Mendoza, M.; Mendes, R. F.; Barbosa, P.; Figueiredo, F.; Figueira, F.; Almeida Paz, F. A.; Delgado-López, J. M.; Rodríguez-Diéguez, A.; Seco, J. M.; Adsorptive, Capacity, Inhibitory Activity and Processing Techniques for a Copper-MOF Based on the 3,4-Dihydroxybenzoate Ligand. *Molecules* **2022**, *27* (22). DOI: 10.3390/molecules27228073.

(36) Palatinus, L.; Petříček, V.; Correâ, C. A. Structure Refinement Using Precession Electron Diffraction Tomography and Dynamical Diffraction: Theory and Implementation. *Acta Crystallogr. A Found Adv.* **2015**, *71*, 235−244.

(37) Klimakow, M.; Klobes, P.; Thünemann, A. F.; Rademann, K.; Emmerling, F. Mechanochemical Synthesis of Metal-Organic Frameworks: A Fast and Facile Approach toward Quantitative Yields and High Specific Surface Areas. *Chem. Mater.* **2010**, *22* (18), 5216−5221.

(38) Palatinus, L.; Brázda, P.; Jelínek, M.; Hrdá, J.; Steciuk, G.; Klementová, M. Specifics of the Data Processing of Precession Electron Diffraction Tomography Data and Their Implementation in the Program PETS2.0. *Acta Crystallogr. B Struct Sci. Cryst. Eng. Mater.* **2019**, *75*, 512−522.

(39) Sheldrick, G. M. SHELXT - Integrated Space-Group and Crystal-Structure Determination. *Acta Crystallogr. A* **2015**, *71* (1), 3−8.

(40) Petříček, V.; Palatinus, L.; Plášil, J.; Dušek, M. J Ana 2020 - a New Version of the Crystallographic Computing System J Ana. *Z. Kristallogr Cryst. Mater.* **2023**. 238271.

(41) MacRae, C. F.; Sovago, I.; Cottrell, S. J.; Galek, P. T. A.; McCabe, P.; Pidcock, E.; Platings, M.; Shields, G. P.; Stevens, J. S.; Towler, M.; Wood, P. A. Mercury 4.0: From Visualization to Analysis, Design and Prediction. *J. Appl. Crystallogr.* **2020**, *53*, 226−235.

(42) Schoedel, A.; Li, M.; Li, D.; O'Keeffe, M.; Yaghi, O. M. Structures of Metal-Organic Frameworks with Rod Secondary Building Units. *Chem. Rev.* **2016**, *116*, 12466−12535. American Chemical Society October 12

(43) Klar, P. B.; Krysiak, Y.; Xu, H.; Steciuk, G.; Cho, J.; Zou, X.; Palatinus, L. Accurate Structure Models and Absolute Configuration Determination Using Dynamical Effects in Continuous-Rotation 3D Electron Diffraction Data. *Nat. Chem.* **2023**, *15* (6), 848−855.

(44) Gagné, O. C.; Hawthorne, F. C. Bond-Length Distributions for Ions Bonded to Oxygen: Results for the Transition Metals and Quantification of the Factors Underlying Bond-Length Variation in Inorganic Solids. *IUCrJ.* **2020**, *7*, 581−629.

(45) Müller, P.; Herbst-Irmer, R.; Spek, A. L.; Schneider, T. R.; Sawaya, M. R. *Crystal Structure Refinement*; Oxford University

PressOxford, 2006. DOI: 10.1093/acprof:oso/9780198570769.001.0001.

(46) Yan, C.; Jin, J.; Wang, J.; Zhang, F.; Tian, Y.; Liu, C.; Zhang, F.; Cao, L.; Zhou, Y.; Han, Q. Metal−Organic Frameworks (MOFs) for the Efficient Removal of Contaminants from Water: Underlying Mechanisms, Recent Advances, Challenges, and Future Prospects. *Coord. Chem. Rev.*. Elsevier B.V. October 1, 2022. DOI: 10.1016/j.ccr.2022.214595.

(47) Lellis, B.; Fávaro-Polonio, C. Z.; Pamphile, J. A.; Polonio, J. C. Effects of Textile Dyes on Health and the Environment and Bioremediation Potential of Living Organisms. *Biotechnology Research and Innovation* **2019**, *3* (2), 275−290.

(48) Oladoye, P. O.; Ajiboye, T. O.; Omotola, E. O.; Oyewola, O. J. Methylene Blue Dye: Toxicity and Potential Elimination Technology from Wastewater. *Results in Engineering*. Elsevier B.V. December 1, 2022. DOI: 10.1016/j.rineng.2022.100678.